JHAD
Health and Development Journal
https://jhad.kmu.ac.ir
10.34172/jhad.92360
Vol. 13, No. 1, 2024, 1-10

Original Article

Optimization of Vancomycin Antibiotic Removal from Synthetic and Real Wastewater Using UV/Fe_3O_4@Alg-ZnO Nanocomposite Photocatalysis: Response Surface Methodology Based on a Box-Behnken Design

Mahsa Rahrovan[1], Hasan Rahmani[1*], Davarkhah Rabbani[1], Mohammadbagher Miranzadeh[1], Habibollah Rahimi[2]

[1]Department of Environmental Health Engineering, School of Health, Kashan University of Medical Sciences, Kashan, Iran
[2]Department of Biostatistics and Epidemiology, School of Public Health, Kashan University of Medical Sciences, Kashan, Iran

***Corresponding Author:** Hasan Rahmani, Email: hs.rahmani@yahoo.com

Abstract

Background: Vancomycin (VCM) is a critical antibiotic due to its high consumption and side effects, including increased bacterial resistance affecting treatment processes. This research investigated the efficiency of VCM antibiotic removal from an aqueous solution using a UV/Fe_3O_4@Alg-ZnO integrated process.

Methods: Response surface methodology (RSM) and a Box-Behnken design were applied using Design-Expert software to optimize the number of samples and simultaneously understand the interactive effects between variables. X-ray diffraction (XRD), a vibrating-sample magnetometer (VSM), field effect scanning electron microscopy (FE-SEM), and Fourier transform infrared (FTIR) analyses were used to check the structural characteristics. The effects of initial catalyst concentration (0.1, 0.3, and 0.5 g/L), initial pollutant concentration (10, 30, and 50 mg/L), contact time (10, 30, and 50 minutes), and pH (3, 7, and 11) on VCM decomposition rate were investigated. Spectrophotometry, total organic carbon (TOC), and GC-MS analyses were used to check the efficiency of the process.

Results: In this study, VCM and TOC removal efficiency was 92.64% and 85.38%, respectively, under optimal conditions. The reason for the reduction in the efficiency of the combined UV/Fe_3O_4@Alg-ZnO process in real raw sewage, after activated sludge (13%) and after activated sludge and stabilization ponds (24%), is the high COD, which causes the active radicals produced to be spent on other species instead of the VCM antibiotic.

Conclusion: The current study showed that the UV/Fe_3O_4@Alg-ZnO process performs well in removing VCM and TOC. In real wastewater, this efficiency was significantly reduced.

Keywords: Photocatalysis, Vancomycin antibiotic removal, Wastewater, UV/Fe_3O_4@Alg-ZnO, Response surface methodology

Citation: Rahrovan M, Rahmani H, Rabbani D, Miranzadeh M, Rahimi H. Optimization of vancomycin antibiotic removal from synthetic and real wastewater using UV/Fe_3O_4@Alg-ZnO nanocomposite photocatalysis: response surface methodology based on a box-behnken design. Health Dev J. 2024;13(1):1–10. doi:10.34172/jhad.92360

Received: November 21, 2023, **Accepted:** February 12, 2024, **ePublished:** February 27, 2024

Introduction

The global consumption of antibiotics ranges from 100 000–200 000 tons per year (1). About 30%–90% of antibiotics enter aquatic environments without being metabolized through body waste, medical waste, medical livestock, industries, etc. These drugs have been found in different concentrations, from nanograms to micrograms, in drinking water, domestic sewage, and surface and underground water (2,3). These findings show that antibiotics are incompletely decomposed in treatment plants and can enter receiving waters (4,5). Antibiotics have increased bacterial resistance, which is considered a threat to the health of humans and other organisms. Also, their presence in the sewage system disrupts the activity of sewage treatment bacteria (6,7). The antibiotic vancomycin (VCM) was first identified in 1950. This antibiotic is a beta-lactam-glycopeptide antibiotic used to treat gram-positive bacterial infections (8). Due to the complex structure of drugs, conventional processes for treating water and wastewater cannot decompose and remove these compounds. Biological treatment is ineffective in removing these compounds due to the low reaction speed, the need for sludge disposal, accurate control of pH and temperature, and the removal of effective bacteria by antibiotics in the treatment. Also, physical methods are not efficient enough. Chemical treatment also leads to the production of harmful byproducts (4,9,10). Advanced oxidation

processes (AOPs) are suitable for removing antibiotics from aqueous solutions. These environmentally friendly processes oxidize and mineralize a wide range of organic pollutants by forming active radicals with high reactivity. Photocatalysis with semiconductors is one of the AOPs with high oxidation potential (11-14). In photocatalytic processes, a semiconductor is used as a catalyst, and UV radiation excites the catalyst electrons. The excited electrons produce hydroxyl radicals (^{o}OH) through various reactions (15-17). These radicals effectively break down organic compounds into their simpler and often less toxic structures. Among the AOPs, ultrasound/hydrogen peroxide, ozonation, O_3/UV, O_3/H_2O_2 and O_3/H_2O_2/UV as hydrogen peroxide-based methods (e.g., H_2O_2/UV, Fenton, Fenton-like, hetero-Fenton, and photon-Fenton), and heterogeneous photocatalysis (TiO_2/UV and TiO_2/H_2O_2/UV systems) can be used for oxidative degradation of organic pollutants and their conversion to products such as carbon dioxide and water in various environmental contexts (18-22). Several heterogeneous catalysts used in photocatalysis include metal oxides (Al_2O_3, MnO_2, CeO_2, and TiO_2), zeolites modified with metals, and metals supported on media such as activated carbon (23,24). Zinc oxide (ZnO) is a semiconductor used to decompose water pollutants. ZnO nanoparticles are low-cost, non-toxic, stable, and highly photosensitive and excitable under sunlight. This nanoparticle has an energy gap of 3.2 eV, which absorbs a large part of the energy of the UV spectrum and has the highest absorption in the wavelength range of 360 to 385 nm (25,26). ZnO nanoparticles tend to accumulate, reducing their contact surface and making it difficult to separate them from the environment. Studies have shown that using the nanoparticles in combination with oxidizing substances can increase their efficiency. Using iron oxide combined with a catalyst is a suitable method for destroying pollutants. Magnetite (Fe_3O_4) is the usual form of magnetic iron oxide, which increases the efficiency of photocatalytic activity due to features such as high surface-to-weight ratio, high density of reaction sites, chemical stability, non-formation of polycyclic products, reduction of recombination of produced electrons and holes, prevention of catalyst escape, and rapid oxidation of pollutants, (27,28). Various materials are used to increase the stabilization of catalysts to improve efficiency. Sodium alginate with the chemical formula $(C_6H_7O_6Na)_n$ is a natural biopolymer that is extracted from a type of brown algae. Due to its availability, compatibility with hydrophobic molecules, non-toxicity, adhesive strength, and suitable mechanical properties, this material is used to create the necessary substrate to prevent the escape of nanoparticles (29). This study's main innovation and objective is the modification of ZnO with Fe_3O_4 and Alg to improve the degradation and mineralization of the antibiotic VCM.

Materials and Methods

Reagents

VCM (CAS Number: 1404-93-9), sodium salt of alginic acid from brown algae ($C_6H_7O_6Na$, with medium viscosity, CAS number: 9005-38-3), iron oxide Fe_3O_4 nanopowder/nanoparticles (Fe_3O_4, 98 + %, 20–30 nm) and zinc oxide (ZnO) (CAS Number: 1314-13-2; Catalog No.: 8849) were acquired from Merck, Germany. A solution (0.01 N) of H_2SO_4 and NaOH available in the laboratory was used to determine the pH conditions of the samples.

Preparation and characterization of the catalyst

First, 1 g of Fe_3O_4 nanoparticles was dissolved in 100 mL of 2.5 g/L sodium alginate solution, and the mixture was subjected to ultrasonic waves for 30 minutes. Then 0.5 gr of ZnO was added to the mixture and subjected to ultrasonic waves for 30 minutes. To prepare samples, a small amount of the solid sample was dispersed in ethanol, and small drops of the solution were placed on an aluminum grid. The grid was dried for 1–2 hours in a vacuum oven at 40 °C. X-ray diffraction (XRD) analysis (model, PertPro used a Cu-Ka beam, copper-cathode) was used to determine the structure and crystalline phase of nanoparticles. Vibrating-sample magnetometer (VSM) analysis was used to compare the magnetic properties of Fe_3O_4 nanoparticles and Fe_3O_4@Alg-ZnO catalyst, and FT-IR analysis was used to determine their structural characteristics. FESEM was carried out using a Hitachi S-4800 microscope.

Experimental procedure

Photocatalytic experiments were conducted in a batch reactor system and on a laboratory scale. A low-pressure UVA mercury lamp (6 W) was placed vertically inside the quartz reactor chamber with a volume of 300 mL. VCM antibiotic solution, in addition to the Fe_3O_4@Alg-ZnO nanocomposite, was placed in the reactor and subjected to ultraviolet radiation and photodegradation. To increase the contact surface of the catalyst and the pollutant, the solution inside the reactor was thoroughly stirred by a mechanical stirrer (South Korea-MS300HS) to prevent the deposition of the nanocomposite on the bottom of the reactor. A VCM stock solution with a concentration of 100 mg/L was prepared synthetically to perform the experiments. This stock solution was used to prepare samples with specific concentrations (10, 30, and 50 mg/L). The prepared samples with specific concentrations were poured into the beaker, and then the pH of the solution was adjusted using (0.01 N) H_2SO_4 and NaOH and a pH meter at room temperature (25 °C) in the range of 3, 7, and 11. Samples were poured into the reactor in order, and specific doses of catalyst (0.1, 0.3, and 0.5 g/L) were added to the reactor. The contents were exposed to a UVA lamp (Philips 244855 UV 6W) and mixed using a stirrer. The reaction times of 10, 30, and 50

minutes were tested. After conducting the experiments, Fe_3O_4 nanoparticles were separated from the solution by a Tesla magnet, and the samples were evaluated by a spectrophotometer (UV-1900i, Shimadzu) to determine the VCM removal efficiency. The total organic carbon (TOC) reduction rate was also measured under optimal conditions, and the metabolites produced during VCM degradation were analyzed by a GC-MS device with Agilent 6890 and MS 5973N (made in the USA) with a DB-5MS column 60 meters long.

Analytical methods

In order to determine the VCM removal efficiency, the absorbance of the samples was measured after centrifugation by a UV-Vis spectrophotometer equipped with a quartz cell (Apel model, PD/uv303) with a wavelength of 280 nm.

VCM removal efficiency was calculated according to Equation 1, where *R* is VCM removal percentage (%), C_0 is the primary concentration of VCM (mg/L), and C_e is the secondary concentration of VCM (mg/L).

$$R = \frac{C_0 - C_e}{C_0} \times 100 \qquad (1)$$

RSM model

In this study, the sample size, the number of tests, the determination of pollutant removal efficiency, and the relationship between variables were determined using RSM (response surface methodology) and a Box-Behnken design. In this method, considering four factors, three levels (low, middle, and high) for each factor, coded as + 1, 0, and -1 (Table 1), and one replication for each experiment, 29 Runs were obtained by Design-Expert software, which is presented in Table 1. These factors include catalyst concentration (0.1, 0.3, and 0.5 g/L), initial pollutant concentration (10, 30, and 50 mg/L), pH (3, 7, and 11), and contact time (10, 30, and 50 minutes).

Results

Characterization of Fe_3O_4@Alg-ZnO nanocomposite

The characterization, surface morphology, and distribution of Fe_3O_4@Alg-ZnO nanocomposite were studied using the field effect scanning electron microscopy (FE-SEM) technique (Figure 1).

The results of the XRD test showed that ZnO has a hexagonal crystal structure, iron oxide is magnetic, and its crystal type is rhombohedral. The intensity of the peaks shows that doping with iron and placing it instead of Zn destroys the crystal structure to some extent. As shown in Figure 2a, the XRD patterns for ZnO sample No. 0075-080-01 and iron oxide No. 1165-087-01 are consistent with their standard card; no additional peak is observed, which shows the purity of ZnO. Diffraction peaks confirm the synthesized Fe_3O_4@Alg-ZnO nanocomposite structure (30). Figure 2b shows the graph obtained from the VSM analysis. The graph showed that the magnetic property of Fe_3O_4@Alg-ZnO nanocomposite (66.7 emu/g) has been slightly reduced compared to Fe_3O_4 nanoparticles (68.9 emu/g) (31).

The results of the FT-IR analysis are given in Figure 3a in relation to the Fe_3O_4@Alg-ZnO nanocomposite spectrum and in Figure 3b in relation to the Fe_3O_4 nanoparticle spectrum. In examining Figure 3a, the peak at 3380.06 cm^{-1} shows O-H stretching vibrations. The band formed in peak1 2920.66 cm is also related to C-H stretching vibrations, which indicates the carbon chain in the Alg molecule used in nanocatalyst synthesis. According to Waldron, ferrites can be considered crystals with continuous bonds (32), i.e., atoms are bound with an equal force (ionic, covalent, or Van der Waals force). The 1643.05 cm^{-1} peak can be related to the stretching vibrations of $COOH^-$ or C=O or due to the H-O-H bond caused by water molecules adsorbed on the surface, which indicates the attraction of the surface of iron oxide nanoparticles to the hydroxyl group and ultimately the dependence between the core Fe_3O_4 and the ZnO shell. The 1387.53 cm^1 peak is related to C=O or O-H, the 1424.17 cm^{-1} to $COOH^-$ or C=O, the 1252.54 cm^{-1} peak to C-O, the 1146.47 cm^{-1} peak to O-H, and the 87.1027 cm^{-1} peak to C-O and O-H. The 874.56 cm^{-1} peak is due to Zn-C bonding, and the 815.742 cm^{-1} peak is related to Zn-C or Zn-OH due to ZnO and alginate bonding. Also, the 539.007 cm^{-1} peak shows the stretching vibrations related to the Fe-O bond caused by Fe_3O_4 (33).

Modeling and statistical analysis

ANOVA analysis, shown in Table 2, was used for statistical analysis. These values were obtained by Design-Expert software for the linear regression model and used to optimize VCM removal. This analysis shows that the selected model significantly affects the photocatalytic process and that the dependent variables significantly affect the removal efficiency. Before determining the model, the necessity of any type of "transformation" in

Table 1. Descriptive characteristics and levels of measured independent variables

Factor	Name	Units	Min	Max	Coded Low	Coded High	Mean
A	pH	-	3.00	11.00	-1 ↔ 3.00	+1 ↔ 11.00	7.00
B	Time	min	10.00	50.00	-1 ↔ 10.00	+1 ↔ 50.00	30.00
C	VAC	ppm	10.00	50.00	-1 ↔ 10.00	+1 ↔ 50.00	30.00
D	Cata	g/L	0.1000	0.5000	-1 ↔ 0.10	+1 ↔ 0.50	0.3000

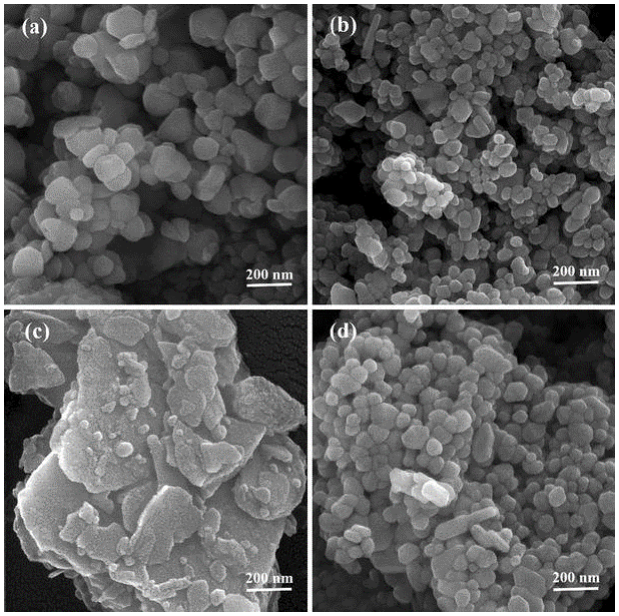

Figure 1. FE-SEM images: (a) Fe_3O_4@Alg-ZnO nanocomposite (1:10), (b) Fe_3O_4@Alg-ZnO nanocomposite (1:20), (c) Fe_3O_4 and (d) ZnO nano crystallite

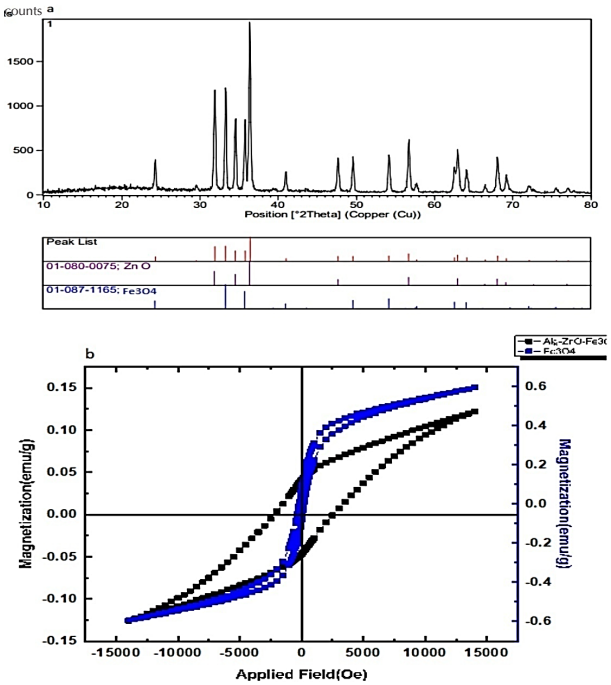

Figure 2. Characterization of Fe_3O_4@Alg-ZnO nanocomposite: (a) XRD and (b) VSM

the comparisons of independent variables was checked using the Box-Cax diagram, the results of which are as follows:

Based on the obtained results, there was no need to convert the observed values. Then, among the different linear, quadratic, and cubic models, a model was proposed based on the R^2 value. Based on the findings related to the fit of the models, the linear model had the highest R^2 and predicted R^2. The results showed that the model had a

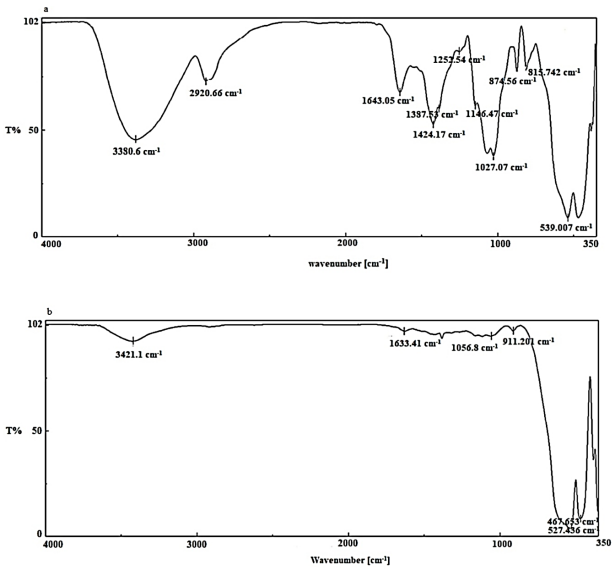

Figure 3. FTIR spectra of (a) the Fe_3O_4@Alg-ZnO nanocomposite and (b) Fe_3O_4 nanoparticles

Table 2. ANOVA for linear model

Source	Sum of squares	df	Mean Square	F-value	*P* value	Significancy
Model	9347.10	4	2336.78	8.04	0.0003	Significant
A-pH	2713.52	1	2713.52	9.34	0.0054	
B-Time	2766.71	1	2766.71	9.52	0.0051	
C-VAC	3736.86	1	3736.86	12.86	0.0015	
D-Cata	130.02	1	130.02	0.4474	0.5099	
Residual	6974.21	24	290.59			
Lack of Fit	6947.28	20	347.36	51.59	0.0008	Significant
Pure Error	26.93	4	6.73			
Cor Total	16321.32	28				

good fit. The high value of R^2 (0.93) shows that the model has good validity, there is a good correlation between the experiment results, and only 6.56% of the total variation is not explained by this model. The closeness of the adjusted R^2 value (0.92) to the R^2 value (0.93) shows that the model has high significance. The difference between the predicted R^2 value (0.89) and the Adjusted R^2 value (0.92) is less than 0.2, which is favorable and significant. The coefficient of variance (CV) (0.16) value shows the test's reliability and the model's repeatability. The value of adequate precision (35.03), which measures the signal-to-noise ratio, is in the acceptable range (4 and above) and shows that the model has high accuracy. The low standard deviation (SD = 8.40) shows that the selected model fits the experimental data.

The results also show that the *P* value is not significant above 0.1; the *P* value of 0.003 shows the statistical significance of the model. The *F*-value of 8.04 emphasizes the significance of the model in removing VCM. Response (R^1) and independent variables (*A*, *B*, *C*, and *D*) can be related to a second-order regression model according to

equation 2. The system's behavior can be explained based on this equation. According to the coefficient of each factor in this equation, it is possible to predict the relative effect of that factor on the amount of removal.

$$R^1 = 58.658 - 15.0375A + 15.1842B - 17.6467C + 3.29167D + 13.0775AB + 13.99AC - 2.36AD - 4.415BC + 4.01BD + 1.575CD - 0.0848333A^2 - 2.23233B^2 - 4.52858C^2 - 3.61108D^2 \quad (2)$$

Therefore, by removing the coefficients that are not significant, equation 2 can be rewritten as equation 3.

$$R^1 = 58.65 - 15.04A + 15.18B - 17.65C + 3.29D \quad (3)$$

In equation 3, R^1 is the percentage of VCM removal, and A, B, C, and D are coded variables related to pH, time, pollutant concentration, and catalyst concentration, respectively.

In order to check the fitness of determined model, the predicted values of model were depicted on y axis versus the actual values on the other axis of graph. In case of ideal goodness-of-fit, the predicted values should be in concordance with the actual one, so they are arranged on a straight line diagonally. Respect to Figure 4a except to the extreme lower and upper values, in overall almost points are near to diagonal line, appropriate goodness-of-fit. Figure 4b shows standardized (Z-score) difference between predicted and actual values. This graph checks any systematic deviation from zero value as the concordance between actual and predicted value by the model, moreover this graph like as graph a. explores any systematic deviation, in cases which there is such deviation in model. As it has shown, there is not any systematic deviation, so the model has enough goodness-of-fit over different values.

The effects of the studied parameters on the efficiency of the UV/Fe_3O_4@Alg-ZnO integrated process

One of the factors affecting the efficiency of the pollutant degradation process is the initial concentration of the pollutant. The present study evaluated VCM pollutant degradation at 10, 30, and 50 mg/L. Referring to Figure 5, the removal efficiency decreases by increasing the pollutant concentration.

To investigate the effect of the initial concentration of the catalyst on the efficiency of the U/Fe_3O_4@Alg-ZnO process, the oxidation process was evaluated with the catalyst concentrations of 0.1, 0.3, and 0.5 g/L. Referring to Figure 5, as the amount of catalyst increases, the VCM removal also increases. The degradation of the VCM antibiotic was evaluated by the UV/Fe_3O_4@Alg-ZnO process at pH values of 3, 7, and 11. Figure 5 shows the three-dimensional diagram of the response surface based on pH and contact time variables. As the pH decreases, the degradation rate increases. The UV/Fe_3O_4@Alg-ZnO process had the highest efficiency at pH = 3.

The reaction time is one of the essential variables for designing and managing an oxidation process. The degradation of the VCM antibiotic was investigated at 10, 30, and 50 minutes to investigate the effect of contact time on the efficiency of the UV/Fe_3O_4@Alg-

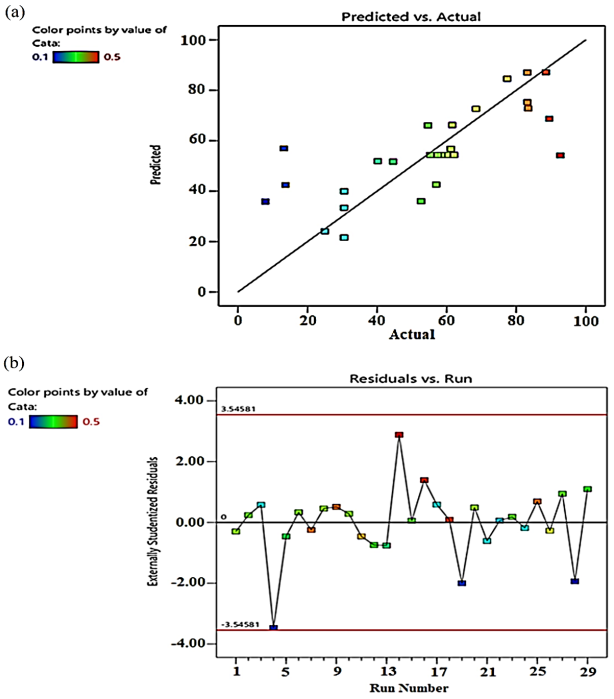

Figure 4. (a) Fit diagram and (b) the distribution diagram of the difference between the predicted value and the actual value based on different runs

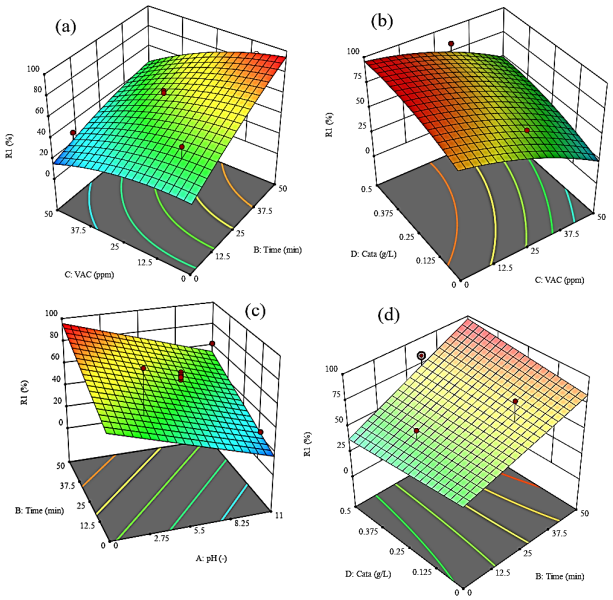

Figure 5. (a). Response surface 3D diagram based on the VCM and time variables (pH = 7, Cata. = 0.3 g/L). (b). Response surface 3D diagram based on the Cata. and VCM variables (pH = 11, Time = 30 min). (c). Response surface 3D diagram based on the pH and contact time variables (VCM = 10 mg/L, Cata. = 0.1 g/L). (d). Response surface 3D diagram based on the Cata. and contact time variables (pH = 7, VCM = 10 mg/L).

ZnO photocatalytic process. According to Figure 5, there is a strong and significant relationship between UV irradiation time and photocatalytic activity, and changes in contact time have a positive correlation with removal efficiency.

As stated below, the amount of electrical energy the UV lamp consumes to remove VCM in each test period was obtained from the following equation.

$$EE/O = \frac{P \times (t/3600) \times 3785}{V \times \log(C_0/C)} \quad (4)$$

That:

P: lamp power (kW); *t*: reaction time(s); *V*: reactor volume (L); C_0: initial concentration of VCM before contact; and *C*: concentration of VCM after exposure.

The results related to the amount of electrical energy consumed during the photocatalytic process are given in Table 3.

The effective parameters in calculating the energy consumption are the power of the UV lamp, the contact time, the reactor's volume, and the precursor's initial concentration before and after the process. Since the integration process in optimal conditions caused the removal of more VCM (92.64%), this issue increased the system's efficiency due to the energy consumed by the UV lamp.

In the next stage of the study, the photocatalytic efficiency of UV/Fe_3O_4@Alg-ZnO for VCM degradation in real wastewater was investigated (two different matrices were selected). Real raw wastewater along with secondary effluent from a wastewater treatment plant of Kashan University of Medical Sciences after activated sludge (COD = 300 mg/L, TDS = 122 mg/L, and pH = 7.85) and stabilization ponds (COD = 200 mg/L, TDS = 101 mg/L, and pH = 8.22) were used for VCM degradation. After centrifugation at 3000 rpm and passing through a 0.2-micron filter, the samples were evaluated under optimal reaction conditions. Then, 30 mg/L VCM was added to the solution. The results of investigating the removal process of VCM in two matrices showed that the UV/Fe_3O_4@Alg-ZnO process can degrade VCM even in complex conditions if enough time is provided to complete the reactions.

Using a TOC analyzer, VCM mineralization was studied by measuring TOC under the optimal conditions of Catalyst = 0.3 g/L, VCM = 30 mg/L, pH = 3, and time = 10 minutes (Figure 6). The TOC removal efficiency was 85.38%. This result shows that the UV/Fe_3O_4@Alg-ZnO process can convert a high percentage of TOC into minerals (water and CO_2). VCM degradation metabolites during the UV/Fe_3O_4@Alg-ZnO process were analyzed by a GC-MS device with Agilent 6890, MS 5973N (made in the USA) with DB-5MS column 60 meters long, which is shown in Figure 7.

Table 3. Measurement of vancomycin removal percentage in 29 runs by the spectrophotometry device (vancomycin removal efficiency)

Run	Factor 1 A: pH	Factor 2 B: Time (min)	Factor 3 C: VAC (ppm)	Factor 4 D: Cata (g/L)	Response1 R_1 (%)	EE/O (kw)
1	7	50	30	0.1	61.6	157.0
2	7	30	30	0.3	28.4	283.7
3	11	30	50	0.3	30.5	283.7
4	11	30	10	0.3	13.2	1135.0
5	3	30	50	0.3	44.6	162.1
6	7	30	30	0.3	60.0	103.2
7	3	30	10	0.3	83.3	49.3
8	7	30	30	0.3	62.1	94.6
9	7	30	10	0.5	83.2	49.3
10	7	30	10	0.3	61.2	31.5
11	3	50	30	0.3	77.4	99.1
12	3	30	30	0.1	54.6	113.5
13	7	50	50	0.3	40.2	314.0
14	3	10	30	0.3	92.6	126.0
15	7	30	30	0.3	45.2	162.1
16	7	30	10	0.1	89.5	39.1
17	7	10	50	0.3	30.5	94.5
18	7	50	10	0.3	88.5	67.2
19	7	10	30	0.5	13.7	378.0
20	11	50	30	0.3	62.0	157.0
21	7	30	50	0.5	30.5	283.7
22	11	10	30	0.3	25.0	126.0
23	7	30	30	0.3	39.4	189.1
24	7	30	50	0.1	30.5	283.7
25	7	50	30	0.5	83.4	81.9
26	3	30	30	0.5	68.4	75.6
27	11	30	30	0.5	57.0	113.5
28	7	10	30	0.1	7.9	378.0
29	11	30	30	0.1	52.6	126.1

Discussion

The present study evaluated VCM pollutant degradation at 10, 30, and 50 mg/L. Increasing the pollutant concentration decreases removal efficiency because the pollutant molecules prevent ultraviolet radiation from reaching the catalyst. As a result, the production of °OH on the catalyst surface decreases. Also, °OH has a greater tendency to participate in side reactions with intermediate products resulting from high pollutant concentrations. On the other hand, the number of active °OH and the number of pollutant molecules is proportional, which is another factor affecting the efficiency of the process at higher concentrations. Because of the specific and constant capacity of the catalyst in producing active °OH, more time is needed to destroy and remove VCM molecules. The result of the present study was consistent with the study of Kaur et al for removing ciprofloxacin

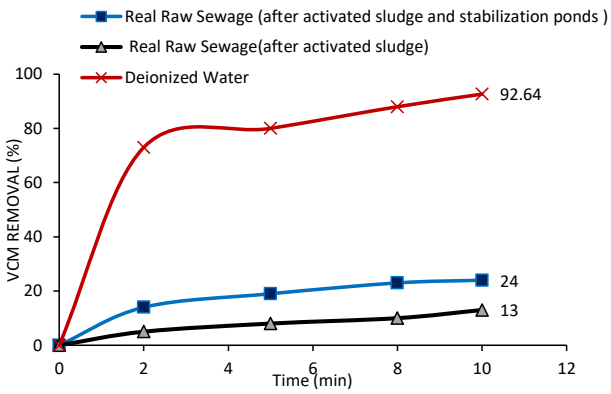

Figure 6. VCM degradation in different aquatic environments (VCM = 30 mg/L, Catalyst = 0.3 g/L, and UV = 6W)

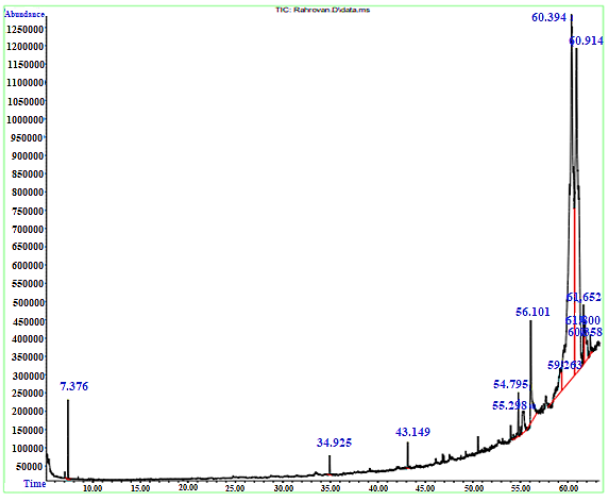

Figure 7. GC-MS analysis diagram of vancomycin after photocatalytic degradation during the UV/Fe_3O_4@Alg-ZnO process

with the silver/iron oxide/ZO photocatalytic process (34). Also, in the study of Das et al on ciprofloxacin removal by the photocatalytic process of ZnO nanoparticles doped with Fe, the removal efficiency decreased with increasing pollutant concentration (35). Referring to Figure 6, as the amount of catalyst increases, the number of active sites on the surface of the nanocomposite increases, and then maximum photon absorption occurs. As a result, hydroxyl radical production increases, leading to an increase in VCM removal. In the study of Batterjee et al on the degradation of ciprofloxacin with ZnO/UV, it was observed that increasing the catalyst concentration up to the optimum point increased the removal efficiency (36). Debnath et al also confirmed this result in the photocatalytic degradation of amoxicillin by ZnO nanoparticles (37). In these processes, the reason for the decrease in removal efficiency at concentrations higher than the optimum point was the increase in the turbidity caused by catalyst particles. According to the following equations, ZnO has a positive charge at pH = 3, and this pH is known as a point charge (PZC). In acidic pH, the predominant species is $ZnOH_2^+$, while in alkaline pH, the predominant species is ZnO^-.

$$Zn\text{-}OH + H^+ \rightarrow ZnOH_2^+ \quad (5)$$

$$Zn\text{-}OH + OH \rightarrow ZnO^- + H_2O \quad (6)$$

Therefore, the adsorption of VCM, which has a negative charge, occurs more easily on the surface of ZnO, which is positively charged in an acidic environment. On the other hand, in alkaline conditions, ZnO is negatively charged like the VCM surface; therefore, electrostatic repulsion occurs between the two compounds. Also, in alkaline conditions, the catalyst particles tend to clump more. This clumping reduces the active surface and the specific surface of the catalyst and causes the reduction of the production of active °OH (38). In the study of El-Kemary et al on the photocatalytic degradation of ciprofloxacin using ZO nanoparticles, with decreasing pH, the removal efficiency decreased, and pH = 10 was considered optimal because this drug has maximum stability in acidic pH solutions. The COOH group in the structure of the compound is not ionized, and the basic nitrogen is completely protonated (39). In the study conducted by Toloman et al on the photocatalytic degradation of the antibiotic oxytetracycline using copper-doped ZnO-MWCNT nanocomposite based on visible light, the appropriate pH for pollutant degradation was about 6. The removal efficiency was very low at alkaline pH, attributed to the repulsion between the photocatalyst and the pollutant, both negatively charged in alkaline conditions (40). With the increase of time, the amount of production of °OH by the catalyst and the probability of collision of VCM molecules with radicals increases. Chankhanittha and Nanan also proved this result in the photocatalytic degradation of antibiotic ofloxacin by ZnO/Bi_2MoO_6 (41). The reason for reducing the efficiency of the combined UV/Fe_3O_4@Alg-ZnO process in real wastewater is the high COD, in which the active radicals produced are spent on other species and VCM antibiotics. GC-MS analysis was done using Agilent 6890, MS 5973N (made in the USA) with a DB-5MS column 60 meters long to identify intermediate products. From the identified straight chain intermediate products like benzene methyl (inhalation of concentrations higher than 200 ppm causes nausea, headache, memory loss, unconsciousness, and even death (42)), tetradecane (over a long period of exposure, it causes hearing loss, loss of color recognition, memory loss, decreased mental ability, damage to the central nervous system, reproductive system, immune system, kidney, liver, and brain, eye and skin irritation, and in case of swallowing, it causes nausea and vomiting (43)), hexadecane (rare allergic symptoms, i.e., itching, rash, swelling, especially in the face, tongue and throat, difficulty breathing, and severe dizziness (44)), hexadecanoic acid methyl ester (no significant

health effect was found), 10-nonadecenal (no significant health effect was found), 9-octadecenamide (fatigue, constipation, flatulence, nausea, vomiting, loss of appetite, and eye and skin irritation (45)), oleic acid (in some cases, irritation of the respiratory system and mucous membrane and skin allergies (46)) hexadecanoic acid (skin irritation, serious eye irritation, serious eye damage, and respiratory irritation (47)), celidoniol (depression, headache, convulsions, tinnitus, itching, nausea, vomiting, diarrhea, abdominal pain, loss of appetite, inflammation of the oral mucosa, male infertility, mild to moderate liver and kidney failure, severe allergies, asthma, anemia, decrease in hemoglobin levels (48)), deoxy (headache, ringing in the ears, muscle weakness in the face, pain in the mouth or throat, difficulty swallowing, cardiac arrhythmia (49)), 1-chlorooctadecane (No significant health effect was found), pentacosane (no significant health effect was found), eicosane (sudden decrease in night vision, lung and liver damages, skin sensitivity to sunlight and UV rays, the feeling of skin stretching due to dryness of the skin on the face and around the lips, and the risk of causing physical and mental disorders for the fetus (50)), docosane (gastrointestinal symptoms such as nausea, indigestion, and stomach pain (51)), tetracosane (dizziness, irritability, seizures, bradycardia, palpitation and cardiac arrhythmia, hives, itching, nausea, and vomiting (52)), heptadecane (it may be fatal if swallowed and enters the respiratory tract (53)), 9-octadecenoic acid (low blood pressure (54)), and grease (infiltrating the devices and preventing them from functioning correctly and cooling them during operation (55)).

Conclusion

The main goal of this research was to measure the effectiveness of the combined UV/Fe_3O_4@Alg-ZnO process in removing the antibiotic VCM from water environments. In this process, in the optimal conditions of initial catalyst concentration of 0.3 g/L, initial antibiotic concentration of 30 mg/L, contact time of 10 minutes, and pH = 3, VCM and TOC removal efficiency was 92.64% and 85.38%, respectively. All factors were effective in removing VCM, and the most effective factors were the initial concentration of the pollutant and the duration of radiation. This research shows that the UV/Fe_3O_4@Alg-ZnO process is promising for degrading organic compounds such as antibiotics and can be used efficiently for treating wastewater, including hospital wastewater. Considering the formation of byproducts resulting from the decomposition of VCM in 10 minutes, it is suggested that to complete the process, the duration of degradation be increased so that VCM is wholly converted into safe compounds. Also, as it achieves high process efficiency in a short period (10 minutes), this method is practical and applicable in industrial or hospital wastewater treatment. Wastewater toxicity evaluation and economic evaluation are suggested for future studies.

Acknowledgments

This article is the result of the master's degree thesis titled "Assessment of the efficiency of UV/Fe_3O_4@Alg-ZnO integrated process in the removal of the antibiotic VCM from aquatic media." This work was supported by Kashan University of Medical Sciences under the grant IR.KAUMS.NUHEPM.REC.1398.069.

Authors' Contribution

Conceptualization: Hasan Rahmani, Davarkhah Rabbani.
Data curation: Mahsa Rahrovan, Hasan Rahmani.
Formal analysis: Mohammadbagher Miranzadeh.
Funding acquisition: Hasan Rahmani.
Investigation: Mahsa Rahrovan, Hasan Rahmani, Davarkhah Rabbani, Mohammadbagher Miranzadeh.
Methodology: Habibollah Rahimi.
Project administration: Hasan Rahmani, Davarkhah Rabbani, Mohammadbagher Miranzadeh.
Resources: Mahsa Rahrovan, Hasan Rahmani.
Supervision: Hasan Rahmani.
Validation: Davarkhah Rabbani, Mohammadbagher Miranzadeh.
Writing–original draft: Mahsa Rahrovan, Hasan Rahmani, Davarkhah Rabbani, Mohammadbagher Miranzadeh.
Writing–review & editing: Mahsa Rahrovan, Hasan Rahmani, Davarkhah Rabbani, Mohammadbagher Miranzadeh, Habibollah Rahimi.

Competing Interests

The authors declare no conflict of interest.

Funding

This study was funded by Kashan University of Medical Sciences (Grant number: IR.KAUMS.NUHEPM.REC.1398.069).

References

1. Van Boeckel TP, Brower C, Gilbert M, Grenfell BT, Levin SA, Robinson TP, et al. Global trends in antimicrobial use in food animals. Proc Natl Acad Sci U S A. 2015;112(18):5649-54. doi: 10.1073/pnas.1503141112.
2. Baranauskaite-Fedorova I, Dvarioniene J. Management of macrolide antibiotics (erythromycin, clarithromycin and azithromycin) in the environment: a case study of environmental pollution in Lithuania. Water. 2022;15(1):10. doi: 10.3390/w15010010.
3. Shi Y, Liu J, Zhuo L, Yan X, Cai F, Luo W, et al. Antibiotics in wastewater from multiple sources and surface water of the Yangtze River in Chongqing in China. Environ Monit Assess. 2020;192(3):159. doi: 10.1007/s10661-020-8108-6.
4. Huang A, Yan M, Lin J, Xu L, Gong H, Gong H. A review of processes for removing antibiotics from breeding wastewater. Int J Environ Res Public Health. 2021;18(9):4909. doi: 10.3390/ijerph18094909.
5. Malakootian M, Faraji M, Malakootian M, Nozari M. Ciprofloxacin removal from aqueous media by adsorption process: a systematic review and meta-analysis. Desalin Water Treat. 2021;229:252-82. doi: 10.5004/dwt.2021.27334.
6. Gamoń F, Banach-Wiśniewska A, Poprawa I, Cema G, Ziembińska-Buczyńska A. Insight into the microbial and genetic response of anammox biomass to broad range concentrations of different antibiotics: linking performance and mechanism. Chem Eng J. 2023;451(Pt 1):138546. doi: 10.1016/j.cej.2022.138546.
7. Nasiri A, Malakootian M, Ansari Shiri M, Yazdanpanah G, Nozari M. CoFe2O4@methylcellulose synthesized as a

new magnetic nanocomposite to tetracycline adsorption: modeling, analysis, and optimization by response surface methodology. J Polym Res. 2021;28(5):192. doi: 10.1007/s10965-021-02540-y.
8. Aerts R, Herrebout W, Johannessen C. Raman optical activity of the antibiotic vancomycin bound to its biological target. J Raman Spectrosc. 2022;53(7):1220-6. doi: 10.1002/jrs.6347.
9. Langbehn RK, Michels C, Soares HM. Antibiotics in wastewater: from its occurrence to the biological removal by environmentally conscious technologies. Environ Pollut. 2021;275:116603. doi: 10.1016/j.envpol.2021.116603.
10. Uluseker C, Kaster KM, Thorsen K, Basiry D, Shobana S, Jain M, et al. A review on occurrence and spread of antibiotic resistance in wastewaters and in wastewater treatment plants: mechanisms and perspectives. Front Microbiol. 2021;12:717809. doi: 10.3389/fmicb.2021.717809.
11. Ma D, Yi H, Lai C, Liu X, Huo X, An Z, et al. Critical review of advanced oxidation processes in organic wastewater treatment. Chemosphere. 2021;275:130104. doi: 10.1016/j.chemosphere.2021.130104.
12. Titchou FE, Zazou H, Afanga H, El Gaayda J, Ait Akbour R, Nidheesh PV, et al. Removal of organic pollutants from wastewater by advanced oxidation processes and its combination with membrane processes. Chem Eng Process Process Intensif. 2021;169:108631. doi: 10.1016/j.cep.2021.108631.
13. Ghime D, Ghosh P. Advanced Oxidation Processes: A Powerful Treatment Option for the Removal of Recalcitrant Organic Compounds. IntechOpen; 2020.
14. Nozari M, Malakootian M, Jaafarzadeh Haghighi Fard N, Mahmoudi-Moghaddam H. Synthesis of Fe3O4@PAC as a magnetic nano-composite for adsorption of dibutyl phthalate from the aqueous medium: modeling, analysis and optimization using the response surface methodology. Surf Interfaces. 2022;31:101981. doi: 10.1016/j.surfin.2022.101981.
15. Liu H, Wang C, Wang G. Photocatalytic advanced oxidation processes for water treatment: recent advances and perspective. Chem Asian J. 2020;15(20):3239-53. doi: 10.1002/asia.202000895.
16. Khan S, Naushad M, Al-Gheethi A, Iqbal J. Engineered nanoparticles for removal of pollutants from wastewater: current status and future prospects of nanotechnology for remediation strategies. J Environ Chem Eng. 2021;9(5):106160. doi: 10.1016/j.jece.2021.106160.
17. Domingues E, Fernandes E, Gomes J, Martins RC. Advanced oxidation processes perspective regarding swine wastewater treatment. Sci Total Environ. 2021;776:145958. doi: 10.1016/j.scitotenv.2021.145958.
18. Aliramaji S, Zamanian A, Sohrabijam Z. Characterization and synthesis of magnetite nanoparticles by innovative sonochemical method. Procedia Materials Science. 2015;11:265-9. doi: 10.1016/j.mspro.2015.11.022.
19. Goldstein JI, Newbury DE, Michael JR, Ritchie NW, Scott JH, Joy DC. Scanning Electron Microscopy and X-ray Microanalysis. Springer; 2017.
20. Khan H, Berk D. Synthesis, physicochemical properties and visible light photocatalytic studies of molybdenum, iron and vanadium doped titanium dioxide. React Kinet Mech Catal. 2014;111(1):393-414. doi: 10.1007/s11144-013-0637-3.
21. Weidauer C, Davis C, Raeke J, Seiwert B, Reemtsma T. Sunlight photolysis of benzotriazoles - identification of transformation products and pathways. Chemosphere. 2016;154:416-24. doi: 10.1016/j.chemosphere.2016.03.090.
22. Nozari M, Malakootian M, Jaafarzadeh Haghighi Fard N, Mahmoudi-Moghaddam H. Degradation of dibutyl phthalate from synthetic and real wastewater using ultrasound/hydrogen peroxide system. Desalin Water Treat. 2023;291:44-62. doi: 10.5004/dwt.2023.29349.
23. Wang Y, Xie Y, Sun H, Xiao J, Cao H, Wang S. Efficient catalytic ozonation over reduced graphene oxide for p-hydroxylbenzoic acid (PHBA) destruction: active site and mechanism. ACS Appl Mater Interfaces. 2016;8(15):9710-20. doi: 10.1021/acsami.6b01175.
24. Yazdanbakhsh A, Rahmani A, Massoudinejad M, Jafari M, Dashtdar M. Accelerating the solar disinfection process of water using modified compound parabolic concentrators (CPCs) mirror. Desalin Water Treat. 2016;57(50):23719-27. doi: 10.1080/19443994.2016.1138147.
25. Terna AD, Elemike EE, Mbonu JI, Osafile OE, Ezeani RO. The future of semiconductors nanoparticles: synthesis, properties and applications. Mater Sci Eng B. 2021;272:115363. doi: 10.1016/j.mseb.2021.115363.
26. Sharma M, Sondhi H, Krishna R, Srivastava SK, Rajput P, Nigam S, et al. Assessment of GO/ZnO nanocomposite for solar-assisted photocatalytic degradation of industrial dye and textile effluent. Environ Sci Pollut Res Int. 2020;27(25):32076-87. doi: 10.1007/s11356-020-08849-3.
27. Luo H, Zeng Y, He D, Pan X. Application of iron-based materials in heterogeneous advanced oxidation processes for wastewater treatment: a review. Chem Eng J. 2021;407:127191. doi: 10.1016/j.cej.2020.127191.
28. Thi Lan Huong P, Van Quang N, Thi Huyen N, Thu Huong H, Anh Tuan D, Trung Tran M, et al. Efficiency enhancement of photocatalytic activity under UV and visible light irradiation using ZnO/Fe3O4 heteronanostructures. Sol Energy. 2023;249:712-24. doi: 10.1016/j.solener.2022.12.011.
29. Bruchet M, Mendelson NL, Melman A. Photochemical patterning of ionically cross-linked hydrogels. Processes. 2013;1(2):153-66. doi: 10.3390/pr1020153.
30. Deepty M, Srinivas C, Kumar ER, Mohan NK, Prajapat CL, Rao TVC, et al. XRD, EDX, FTIR and ESR spectroscopic studies of co-precipitated Mn-substituted Zn-ferrite nanoparticles. Ceram Int. 2019;45(6):8037-44. doi: 10.1016/j.ceramint.2019.01.029.
31. Iqbal A, Mahmood A, Muhammad Khan T, Ahmed E. Structural and optical properties of Cr doped ZnO crystalline thin films deposited by reactive electron beam evaporation technique. Prog Nat Sci Mater Int. 2013;23(1):64-9. doi: 10.1016/j.pnsc.2013.01.010.
32. Waldron RD. Infrared spectra of ferrites. Phys Rev. 1955;99(6):1727-35.
33. Hamouda RA, Salman AS, Alharbi AA, Alhasani RH, Elshamy MM. Assessment of the antigenotoxic effects of alginate and ZnO/alginate-nanocomposites extracted from brown alga fucus vesiculosus in mice. Polymers (Basel). 2021;13(21):3839. doi: 10.3390/polym13213839.
34. Kaur A, Anderson WA, Tanvir S, Kansal SK. Solar light active silver/iron oxide/zinc oxide heterostructure for photodegradation of ciprofloxacin, transformation products and antibacterial activity. J Colloid Interface Sci. 2019;557:236-53. doi: 10.1016/j.jcis.2019.09.017.
35. Das S, Ghosh S, Misra AJ, Tamhankar AJ, Mishra A, Lundborg CS, et al. Sunlight assisted photocatalytic degradation of ciprofloxacin in water using Fe doped ZnO nanoparticles for potential public health applications. Int J Environ Res Public Health. 2018;15(11):2440. doi: 10.3390/ijerph15112440.
36. Batterjee MG, Nabi A, Kamli MR, Alzahrani KA, Danish EY, Malik MA. Green hydrothermal synthesis of zinc oxide nanoparticles for UV-light-induced photocatalytic degradation of ciprofloxacin antibiotic in an aqueous environment. Catalysts. 2022;12(11):1347. doi: 10.3390/

catal12111347.
37. Debnath P, Sen K, Mondal A, Mondal A, Mondal NK. Insight into photocatalytic degradation of amoxicillin by biofabricated granular zinc oxide nanoparticle: mechanism, optimization and toxicity evaluation. Int J Environ Res. 2021;15(3):571-83. doi: 10.1007/s41742-021-00331-3.
38. Degen A, Kosec M. Effect of pH and impurities on the surface charge of zinc oxide in aqueous solution. J Eur Ceram Soc. 2000;20(6):667-73. doi: 10.1016/S0955-2219(99)00203-4.
39. El-Kemary M, El-Shamy H, El-Mehasseb I. Photocatalytic degradation of ciprofloxacin drug in water using ZnO nanoparticles. J Lumin. 2010;130(12):2327-31. doi: 10.1016/j.jlumin.2010.07.013.
40. Toloman D, Popa A, Stan M, Stefan M, Vlad G, Ulinici S, et al. Visible-light-driven photocatalytic degradation of different organic pollutants using Cu doped ZnO-MWCNT nanocomposites. J Alloys Compd. 2021;866:159010. doi: 10.1016/j.jallcom.2021.159010.
41. Chankhanittha T, Nanan S. Visible-light-driven photocatalytic degradation of ofloxacin (OFL) antibiotic and Rhodamine B (RhB) dye by solvothermally grown ZnO/Bi2MoO6 heterojunction. J Colloid Interface Sci. 2021;582(Pt A):412-27. doi: 10.1016/j.jcis.2020.08.061.
42. Chen CS, Hseu YC, Liang SH, Kuo JY, Chen SC. Assessment of genotoxicity of methyl-tert-butyl ether, benzene, toluene, ethylbenzene, and xylene to human lymphocytes using comet assay. J Hazard Mater. 2008;153(1-2):351-6. doi: 10.1016/j.jhazmat.2007.08.053.
43. Zhang Z, Kleinstreuer C. Deposition of naphthalene and tetradecane vapors in models of the human respiratory system. Inhal Toxicol. 2011;23(1):44-57. doi: 10.3109/08958378.2010.540261.
44. Gifford SP, MacFarlane GR, O'Connor WA, Dunstan RH. Effect of the pollutants lead, zinc, hexadecane and octocosane on total growth and shell growth in the Akoya pearl oyster, *Pinctada imbricata*. J Shellfish Res. 2006;25(1):159-65. doi: 10.2983/0730-8000(2006)25[159:eotplz]2.0.co;2.
45. Sharanakumar TM, Venugopala Reddy KR, Mounesh, Praveen Kumar NY, Suresh, Nandinibaby NH. Investigated aerobic oxidation of aminochlorophenol catalyzed by phthalocyanine complexes. J Indian Chem Soc. 2021;98(10):100139. doi: 10.1016/j.jics.2021.100139.
46. Boelsma E, Tanojo H, Boddé HE, Ponec M. Assessment of the potential irritancy of oleic acid on human skin: evaluation in vitro and in vivo. Toxicol In Vitro. 1996;10(6):729-42. doi: 10.1016/s0887-2333(96)00053-7.
47. Bharath B, Perinbam K, Devanesan S, AlSalhi MS, Saravanan M. Evaluation of the anticancer potential of hexadecanoic acid from brown algae *Turbinaria ornata* on HT-29 colon cancer cells. J Mol Struct. 2021;1235:130229. doi: 10.1016/j.molstruc.2021.130229.
48. Elblehi SS, Hafez MH, El-Far AH. Panax ginseng ameliorates hepatorenal oxidative alterations induced by commercially used cypermethrin in male rats: experimental and molecular docking approaches. Environ Sci Pollut Res Int. 2023;30(50):109702-23. doi: 10.1007/s11356-023-29935-2.
49. Sykes L, MacIntyre DA, Yap XJ, Ponnampalam S, Teoh TG, Bennett PR. Changes in the Th1:Th2 cytokine bias in pregnancy and the effects of the anti-inflammatory cyclopentenone prostaglandin 15-deoxy-Δ(12,14)-prostaglandin J2. Mediators Inflamm. 2012;2012:416739. doi: 10.1155/2012/416739.
50. Kanno S, Furuyama A, Hirano S. Effects of eicosane, a component of nanoparticles in diesel exhaust, on surface activity of pulmonary surfactant monolayers. Arch Toxicol. 2008;82(11):841-50. doi: 10.1007/s00204-008-0306-x.
51. Rizwan K, Khan SA, Ahmad I, Rasool N, Ibrahim M, Zubair M, et al. A comprehensive review on chemical and pharmacological potential of *Viola betonicifolia*: a plant with multiple benefits. Molecules. 2019;24(17):3138. doi: 10.3390/molecules24173138.
52. Uddin SJ, Grice D, Tiralongo E. Evaluation of cytotoxic activity of patriscabratine, tetracosane and various flavonoids isolated from the Bangladeshi medicinal plant *Acrostichum aureum*. Pharm Biol. 2012;50(10):1276-80. doi: 10.3109/13880209.2012.673628.
53. Ogawa K, Futakuchi M, Hirose M, Boonyaphiphat P, Mizoguchi Y, Miki T, et al. Stage and organ dependent effects of 1-O-hexyl-2,3,5-trimethylhydroquinone, ascorbic acid derivatives, n-heptadecane-8-10-dione and phenylethyl isothiocyanate in a rat multiorgan carcinogenesis model. Int J Cancer. 1998;76(6):851-6. doi: 10.1002/(sici)1097-0215(19980610)76:6<851::aid-ijc14>3.0.co;2-5.
54. Tsikas D, Zoerner AA, Jordan J. Oxidized and nitrated oleic acid in biological systems: analysis by GC-MS/MS and LC-MS/MS, and biological significance. Biochim Biophys Acta. 2011;1811(11):694-705. doi: 10.1016/j.bbalip.2011.06.015.
55. Sanghamitra P, Mazumder D, Mukherjee S. Treatment of wastewater containing oil and grease by biological method-a review. J Environ Sci Health A Tox Hazard Subst Environ Eng. 2021;56(4):394-412. doi: 10.1080/10934529.2021.1884468.